CAVITY OF MOLECULAR GAS ASSOCIATED WITH SUPERNOVA REMNANT 3C 397

The Astrophysical Journal, 712:1147–1156, 2010 April 1 doi:10.1088/0004-637X/712/2/1147

CAVITY OF MOLECULAR GAS ASSOCIATED WITH SUPERNOVA REMNANT 3C 397

Bing Jiang[1], Yang Chen[1,2,6], Junzhi Wang[1,2], Yang Su[3], Xin Zhou[1], Samar Safi-Harb[4], and Tracey DeLaney[5]
[1] Department of Astronomy, Nanjing University, Nanjing 210093, China
[2] Key Laboratory of Modern Astronomy and Astrophysics, Nanjing University, Ministry of Education, China
[3] Purple Mountain Observatory, Chinese Academy of Sciences, Nanjing 210008, China
[4] Department of Physics and Astronomy, University of Manitoba, Winnipeg, MB R3T 2N2, Canada
[5] Kavli Institute for Astrophysics and Space Research, Massachusetts Institute of Technology, 70 Vassar Street, Cambridge, MA 02139, USA
Received 2009 September 3; accepted 2010 January 26; published 2010 March 11

ABSTRACT

3C 397 is a radio and X-ray bright Galactic supernova remnant (SNR) with an unusual rectangular morphology. Our CO observation obtained with the Purple Mountain Observatory at Delingha, Qinghai Province, China reveals that the remnant is well confined in a cavity of molecular gas and embedded at the edge of a molecular cloud (MC) at the local standard of rest systemic velocity of ∼32 km s^{-1}. The cloud has a column density gradient increasing from southeast to northwest, perpendicular to the Galactic plane, in agreement with the elongation direction of the remnant. This systemic velocity places the cloud and SNR 3C 397 at a kinematic distance of ∼10.3 kpc. The derived mean molecular density (∼10–30 cm^{-3}) explains the high volume emission measure of the X-ray emitting gas. A ^{12}CO line broadening of the ∼32 km s^{-1} component is detected at the westmost boundary of the remnant, which provides direct evidence of the SNR–MC interaction and suggests multi-component gas there with dense (∼10^4 cm^{-3}) molecular clumps. We confirm the previous detection of an MC at ∼38 km s^{-1} to the west and south of the SNR and argue, based on H I self-absorption, that the cloud is located in the foreground of the remnant. A list of Galactic SNRs presently known and suggested to be in physical contact with environmental MCs is appended in this paper.

Key words: ISM: individual objects (3C 397 (G41.1–0.3)) – ISM: molecules – ISM: supernova remnants

Online-only material: color figures

1. INTRODUCTION

Core-collapse supernovae are often not far away from their natal giant molecular clouds (MCs). About half of the Galactic supernova remnants (SNRs) are expected to be in physical contact with MCs (Reynoso & Mangum 2001), but so far only less than 40 SNR–MC associations have been confirmed (see the Appendix). These associations are mostly established by the detection of OH 1720 MHz masers (e.g., Frail et al. 1996; Green et al. 1997). For the other few cases, the convincing evidence comes from the sub-millimeter/millimeter observations of molecular lines and infrared observations in recent decades, including molecular line broadening, high line ratio (e.g., ^{12}CO $J = 2$–$1/J = 1$–0), morphological correspondence of molecular emission, etc. Many SNR–MC associations may have not yet been revealed mainly because the OH maser emission is below the detection thresholds (Hewitt & Yusef-Zadeh 2009). Even for most of the SNRs whose interaction with MCs are confirmed, the detailed distribution of environmental molecular gas, which can shed light on the SNRs' dynamical evolution and physical properties, is poorly known. In this regard, line emission of CO and its isotopes plays an important role in the study of the SNR–MC association.

3C 397 (G41.1−0.3) is a radio and X-ray bright Galactic SNR with a peculiar rectangular morphology. It is elongated along the southeast (SE)–northwest (NW) direction, perpendicular to the Galactic plane (Anderson & Rudnick 1993). In X-rays, a "hot" spot was detected near the geometric center (Chen et al. 1999; Dyer & Reynolds 1999; Safi-Harb et al. 2000), suggestive of a compact object associated with the SNR; however, using the *ASCA* and *Chandra* observations, no pulsed signal and no hard, non-thermal emission were detected from it as would be expected from a neutron star or a pulsar wind nebula (Chen et al. 1999; Safi-Harb et al. 2000, 2005, hereafter S05). Based on the irregular morphology seen in the radio and X-rays, the sharp western boundary, and the higher density in the western region of the SNR, S05 suggested that SNR 3C 397 is encountering or interacting with a MC to the west. Using millimeter data to study the environs of 3C 397, they found evidence for an MC at a local standard of rest (LSR) velocity of $V_{\rm LSR} = 35$–40 km s^{-1} to the west and south of the remnant, and suggested a possible association between the cloud and the SNR. The non-detection of OH masers toward the SNR and the small ^{12}CO $(J = 2$–$1)/(J = 1$–$0)$ ratio led S05 to conclude that either the MC is in the close vicinity of the SNR but has not yet been overrun by the shock wave, or that if the SNR–MC interaction is occurring, it must be taking place along the line of sight.

Motivated by the above findings and aiming to investigate the detailed distribution of the molecular gas environing SNR 3C 397, we performed a new observation in ^{12}CO ($J = 1$–0) and ^{13}CO ($J = 1$–0) lines toward the remnant. In this paper, we present our discovery of a cavity of molecular gas associated with 3C 397 and argue that the 38 km s^{-1} cloud is likely in the foreground of the SNR.

2. OBSERVATIONS

The observation was taken with the 13.7 m millimeter-wavelength telescope of the Purple Mountain Observatory at Delingha (hereafter PMOD), China, during 2008 November to December. An SIS receiver was used to simultaneously observe the ^{12}CO ($J = 1$–0) line (at 115.271 GHz) and ^{13}CO ($J = 1$–0) line (at 110.201 GHz), while two acousto-optical spectrometers were used as the back end with 1024 channels. The corresponding spectral coverage was 145 MHz for ^{12}CO (J

[6] Author to whom any correspondence should be addressed.

= 1–0) and 43 MHz for ^{13}CO (J = 1–0). We mapped a 4′ × 3.′5 area centered at ($19^h07^m34.^s0$, +07°08′00.″0, J2000.0), which covers 3C 397 via raster-scan mapping with a grid spacing of 30″. The half-power beamwidth of the telescope was 60″ and the main-beam efficiency was 52% during the observation epoch. The typical system temperature was around 180–260 K. The observed LSR velocity ranges were −150 to +230 km s^{-1} for ^{12}CO and −19 to +99 km s^{-1} for ^{13}CO. The velocity resolution was 0.5 km s^{-1} for ^{12}CO and 0.2 km s^{-1} for ^{13}CO. After performing elevation calibration and baseline subtraction with a low-order polynomial fit, we got an average rms noise of ∼0.3 K for both ^{12}CO and ^{13}CO data. All the CO data were reduced using the GILDAS/CLASS package.[7] The quality of the new CO observation is generally similar to that of the SEST and GPS data used in S05, except that the grid points for ^{12}CO (J = 1–0) are set denser than those in the SEST data.

In order to correlate the distribution of molecular material in the environs of 3C 397 with the morphology of the SNR, we used the archival *Chandra* X-ray (ObsID: 1042, PI: S. S. Holt) and *Spitzer* 24 μm mid-infrared (IR) (PID: 3483, PI: J. Rho) data. The VLA 1.4 GHz radio continuum emission (L band) data were adopted from Anderson & Rudnick (1993), and the H I line emission data were obtained from the VLA Galactic Plane Survey (VGPS; Stil et al. 2006).

3. RESULTS

3.1. The Molecular Gas Cavity at V_{LSR} ∼ 32 km s^{-1}

Figure 1 shows the ^{12}CO (J = 1–0) and ^{13}CO (J = 1–0) spectra averaged over the field of view (FOV). Several velocity components are present in the velocity range V_{LSR} = 0–100 km s^{-1}, and no CO emission is detected outside of this range. There are two prominent CO emission peaks around 38 km s^{-1} and 55 km s^{-1}. We made ^{12}CO emission intensity channel maps with ∼1 km s^{-1} velocity intervals. No evidence is found for the positional correlation between the 55 (50–70) km s^{-1} CO component and SNR 3C 397. The other prominent CO emission peak at 38 km s^{-1} appears to form a crescent strip that partially surrounds the western and southern borders of the remnant as shown in the 35–42 km s^{-1} velocity interval of Figure 2. This is consistent with the structure seen in the ^{13}CO images in the 35.4–41.3 km s^{-1} interval found by S05.

Interestingly, the intensity maps in the 27–35 km s^{-1} interval of Figure 2 reveal a "bay"-like cavity of molecular gas that coincides with the remnant well. The SNR appears surrounded by the molecular gas except in the SE. As seen in the CO spectra (Figure 1), the molecular gas in this range corresponds to a molecular component peaked at 32 km s^{-1}. Although not as prominent as the 38 km s^{-1} component, the 32 km s^{-1} component can be resolved in both the ^{12}CO and ^{13}CO spectra. Because ^{13}CO (J = 1–0) is usually optically thin and indicative of a high column density of H_2 molecules, the presence of the ^{13}CO peak ($\gtrsim 6\sigma$) at ∼ 32 km s^{-1} implies that it is not a broadened part from the left wing of the 38 km s^{-1} peak, but a separate component.

Figure 3 shows the integrated ^{12}CO map in the velocity range of 27–35 km s^{-1} overlaid with the *Chandra* 0.5–8 keV X-ray image and the *Spitzer* 24 μm mid-IR image of the SNR. The mid-IR image displays a distinct SNR "shell" in the north, west, and southwest, and has a morphology strikingly similar to that

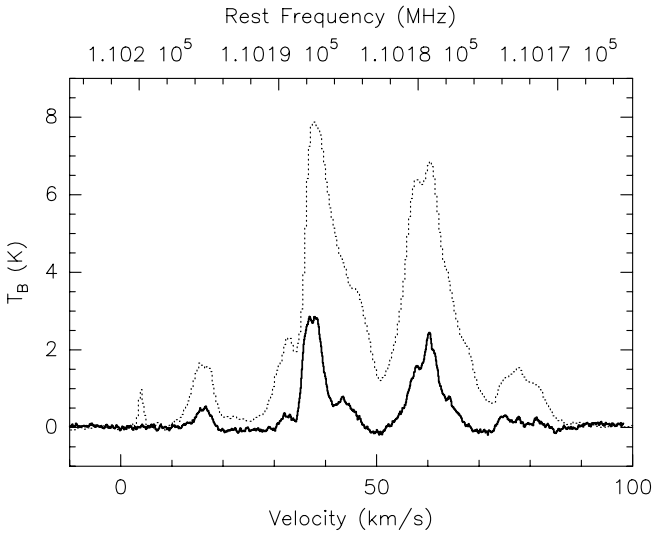

Figure 1. Average CO spectra over the FOV. The dashed line is ^{12}CO (J = 1–0) and the solid line is ^{13}CO (J = 1–0) (multiplied by a factor of 2).

in radio and X-rays. In particular, it is worth noting the sharp western boundary seen at all wavelengths. The box-like shell appears to be well confined in the molecular gas cavity, both of which seem open in the SE. Furthermore, the flat northeastern boundary appears to follow a sharp ^{12}CO intensity interface. This is consistent with a possible density enhancement in the north as suggested by Anderson & Rudnick (1993) for the inhibition of the SNR expansion in this direction.

The 27–35 km s^{-1} ^{12}CO intensity gradient from SE to NW is clearly seen in Figures 2 and 3. This is consistent with the large-scale density gradient which was suggested based on the SNR brightening in radio toward the Galactic plane (Anderson & Rudnick 1993). In order to remove the confusion by this broad structure at low Galactic latitude (−0.°3), we applied the unsharp masking method as described in Landecker et al. (1999) in which we subtracted the smoothed ^{12}CO intensity map (Figure 4, left panel) from the original ^{12}CO map. In the resultant "cleaned" image (Figure 4, right panel), the remnant sits within a ^{12}CO emission void again. A similar result can also be obtained by subtracting the smoothed and scaled ^{13}CO 27–35 km s^{-1} intensity map from the ^{12}CO image. The ^{12}CO emission seems weak along the southwestern border of the SNR in both Figures 3 and 4. This may be because the intensity is integrated only to 35 km s^{-1} (due to the overlap of the left wing of the 38 km s^{-1} component; see Figure 1) so that the contribution from the right wing of the 32 km s^{-1} component is not taken into account. Beyond 35 km s^{-1}, the ^{12}CO emission of the crescent strip (mentioned above) at around 38 km s^{-1} is strong in the southwest (see Figure 2) and does not allow us to unambiguously distinguish the contribution there from the right wing of the 32 km s^{-1} component.

As described above, both the 38 km s^{-1} and the 32 km s^{-1} CO velocity components are shown to have a spatial correlation with SNR 3C 397. By comparison, the morphological correspondence of the former is not as good as the latter because there is no molecular density enhancement in the northeast around 38 km s^{-1} to confine the remnant.

Applying the Milky Way's rotation curve of Clemens (1985) together with R_0 = 8.0 kpc (Reid 1993) and V_0 = 220 km s^{-1}, the systemic LSR velocity of 32 km s^{-1} corresponds to two candidate kinematic distances, 1.7 kpc (near side) and 10.3 kpc (far side). For 38 km s^{-1} the kinematic distances are 2.1 kpc

[7] http://www.iram.fr/IRAMFR/GILDAS

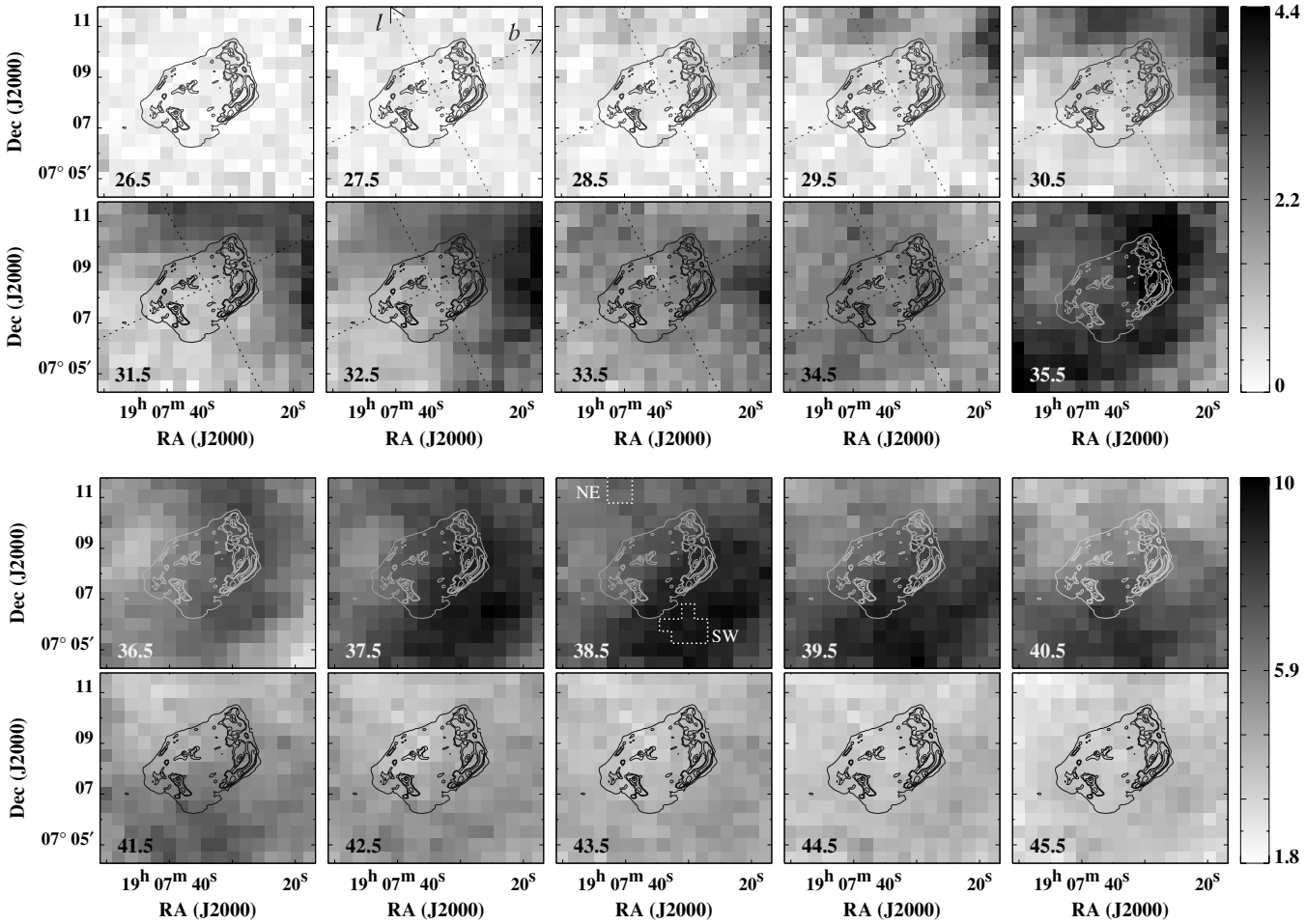

Figure 2. ^{12}CO ($J = 1$–0) intensity maps integrated each 1 km s^{-1} in the velocity range of 26–46 km s^{-1}, overlaid by VLA 1.4 GHz radio continuum emission in contours with levels of 2, 9, 13.5, 18, 23, and 32 mJy beam^{-1}. The central velocities are marked in each image. The average rms noise of each map is 0.18 K km s^{-1}. The dashed boxes labeled with "NE" and "SW" denote the regions from which the ^{13}CO and H I spectra (see Figure 5) were extracted. The dashed lines indicate lines of Galactic latitude and longitude along which the column density distribution $N(H_2)$ of the 32 km s^{-1} ^{12}CO molecular component was derived (see Figure 8).

and 9.9 kpc. For comparison, the tangent point in the direction to 3C 397 is at ∼6.0 kpc. The discrepancy of the kinematic distances to the two molecular components is at least 0.4 kpc, much larger than the typical size of a giant MC complex (∼50 pc; Cox 2000). Thus, it is almost impossible for SNR 3C 397 to simultaneously interact with the two clouds.

We can use the H I self-absorption (SA) measurement to help resolve the near–far ambiguity in kinematic distances, as suggested by Liszt et al. (1981) and Jackson et al. (2002). The likelihood of detecting H I SA favors the geometry in which a cloud lies at the near kinematic distance (see Figure 1 in Roman-Duval et al. 2009 for this reasoning). Figure 5 shows the VGPS H I and PMOD ^{13}CO spectra of the NE and SW regions near the SNR. The H I SA associated with the ^{13}CO peak is clearly seen at 38 km s^{-1}, which indicates that this cloud is most probably at the near distance, 2.1 kpc. On the contrary, little H I SA is detected at 32 km s^{-1}. It has been suggested that SNR 3C 397 is located beyond 7.5 kpc and behind the tangent point based on the H I absorption (Radhakrishnan et al. 1972; Caswell et al. 1975). Therefore, the 38 km s^{-1} velocity component is likely to be a foreground MC toward the SNR.

3.2. Kinematic Evidence for Interaction

A grid of ^{12}CO ($J = 1$–0) spectra is produced focusing on the 32 km s^{-1} component (Figure 6). We inspected the local

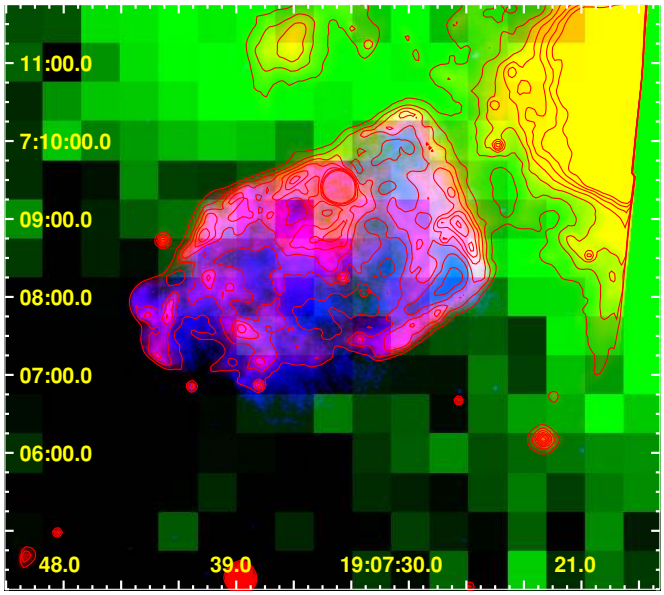

Figure 3. ^{12}CO ($J = 1$–0) intensity map in the velocity interval 27–35 km s^{-1} (above 6σ) coded in green, overlaid with the *Chandra* X-ray image in blue, *Spitzer* 24 μm mid-IR image in red (with seven contours at logarithmic levels between 68 and 120 MJy sr^{-1}). The bright yellow in the northwestern corner shows a part of the foreground H II region G41.096−0.213 at V_{LSR} ∼ 59 km s^{-1}.

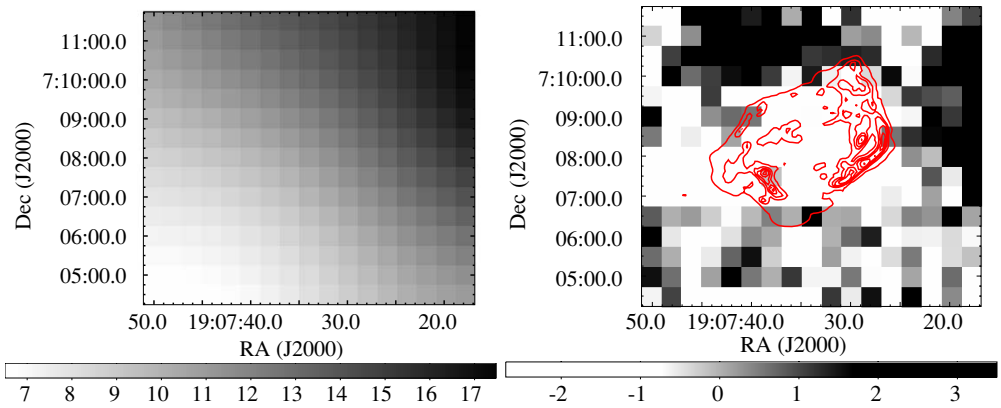

Figure 4. Left panel: the ^{12}CO data intensity map in the same velocity interval as in Figure 3, smoothed to 2.′5 to illustrate the large-scale confusion in this direction. Right panel: the same ^{12}CO data as in Figure 3 after unsharp masking (see the text in Section 3.1), overlaid by VLA 1.4 GHz contours with the same levels as in Figure 2.

(A color version of this figure is available in the online journal.)

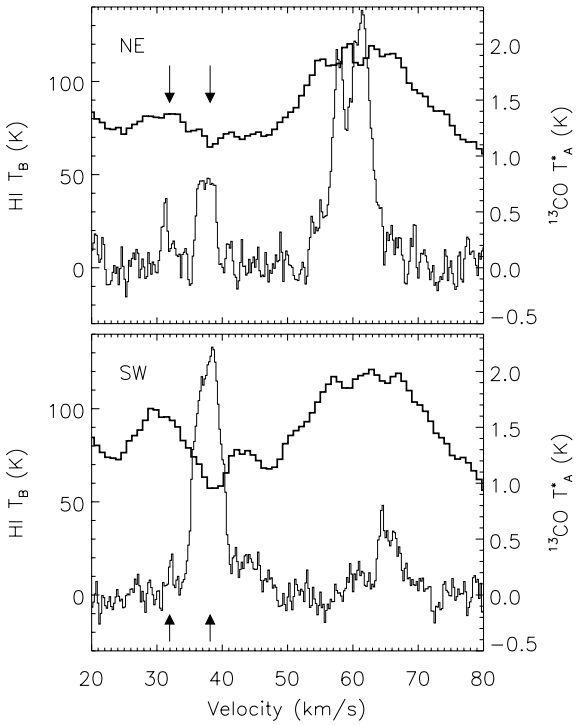

Figure 5. VGPS H I (thick line) and PMOD ^{13}CO (thin line) spectra for the NE (upper panel) and SW (lower panel) regions marked in Figure 2. The arrows denote the locations of the LSR velocities of 32 km s^{-1} and 38 km s^{-1}.

spectra along the edges of the remnant and found that the blue (left) wings (∼28–31 km s^{-1}) of the ^{12}CO line profiles of the 32 km s^{-1} component in the northern, northwestern, and westmost edges (see regions "N," "NW," and "W" marked in Figure 6) appear to be broadened, as shown in Figure 7. The blue wings of other positions along the SNR boundary are not seen to be similarly broadened. In other cases of SNRs such as IC 443 (White et al. 1987), W28 (Arikawa et al. 1999), G347.3−0.5 (Moriguchi et al. 2005), Kes 69 (Zhou et al. 2009), and Kes 75 (Su et al. 2009), the ^{12}CO line broadenings show that the surrounding molecular gas suffers a perturbation and are regarded as strong kinematic evidence for the SNR shock–MC interaction. The broad line profiles seen in 3C 397 are possibly evidence of such an interaction. We cannot conclude whether the red (right) wings of the 32 km s^{-1} lines in the three regions are broad or not, because they are overlapped by the left wings of the strong 38 km s^{-1} lines, which makes it difficult to determine the broadness of the red sides of the 32 km s^{-1} lines.

In the regions "N" and "NW" of 3C 397, the broad left wings may include the contribution from real line broadening due to shock perturbation. In the northern edge of the SNR, there are some X-ray structures that seem to be interacting with the cloud, such as a hat-like Si knot and an S shell (according to the X-ray equivalent line width study in Jiang & Chen 2010). However, we also note that in a wide northern and northeastern area in the FOV (see Figure 6), some ^{12}CO emission peaks at 30 km s^{-1} and thus may more or less contaminate the broad blue wings of line profiles of regions "N" and "NW."

In the westmost region "W," there is a unique plateau in the broad blue wing. No significant ^{12}CO emission at 30 km s^{-1} is seen near this region. Therefore, the broad blue wing can be safely ascribed to Doppler broadening of the 32 km s^{-1} line, which provides solid kinematic evidence of interaction between SNR 3C 397 and the adjacent 32 km s^{-1} MC. It is noteworthy that this westmost line-broadening region is essentially located at a right-angle corner of the rectangular-shaped SNR, which is close to the western radio and X-ray brightness peaks and seems to be coincident with the western end of the Fe-rich ejecta along the "diagonal" as revealed in the X-ray equivalent width maps (Jiang & Chen 2010). Thus, as a possibility, the molecular gas in this region might be impacted by the Fe-rich ejecta.

The fitted and derived parameters for the 32 km s^{-1} molecular component in region "W" are summarized in Table 1. Here we have applied two methods to estimate the H_2 column density and the molecular mass. In the first method, the X-factor $N(H_2)/W(^{12}CO) \approx 1.8 \times 10^{20}$ cm^{-2}K^{-1} km^{-1}s (Dame et al. 2001) is used. In the second one, local thermodynamic equilibrium for the gas and optically thick condition for the ^{13}CO (J = 1–0) line are assumed, and another conversion relation $N(H_2) \approx 7 \times 10^5 N(^{13}CO)$ (Frerking et al. 1982) is used.

In view of the morphological correspondence, the broadened line profile, and the H I SA comparison, we suggest that SNR 3C 397 is associated and interacting with the 32 km s^{-1} MC, which is at a distance of ∼10.3 kpc, and parameterize the distance to the SNR as $d = 10.3 d_{10.3}$ kpc. The distance values used in the previous X-ray studies (e.g., S05) are numerically very similar to the distance determined here.

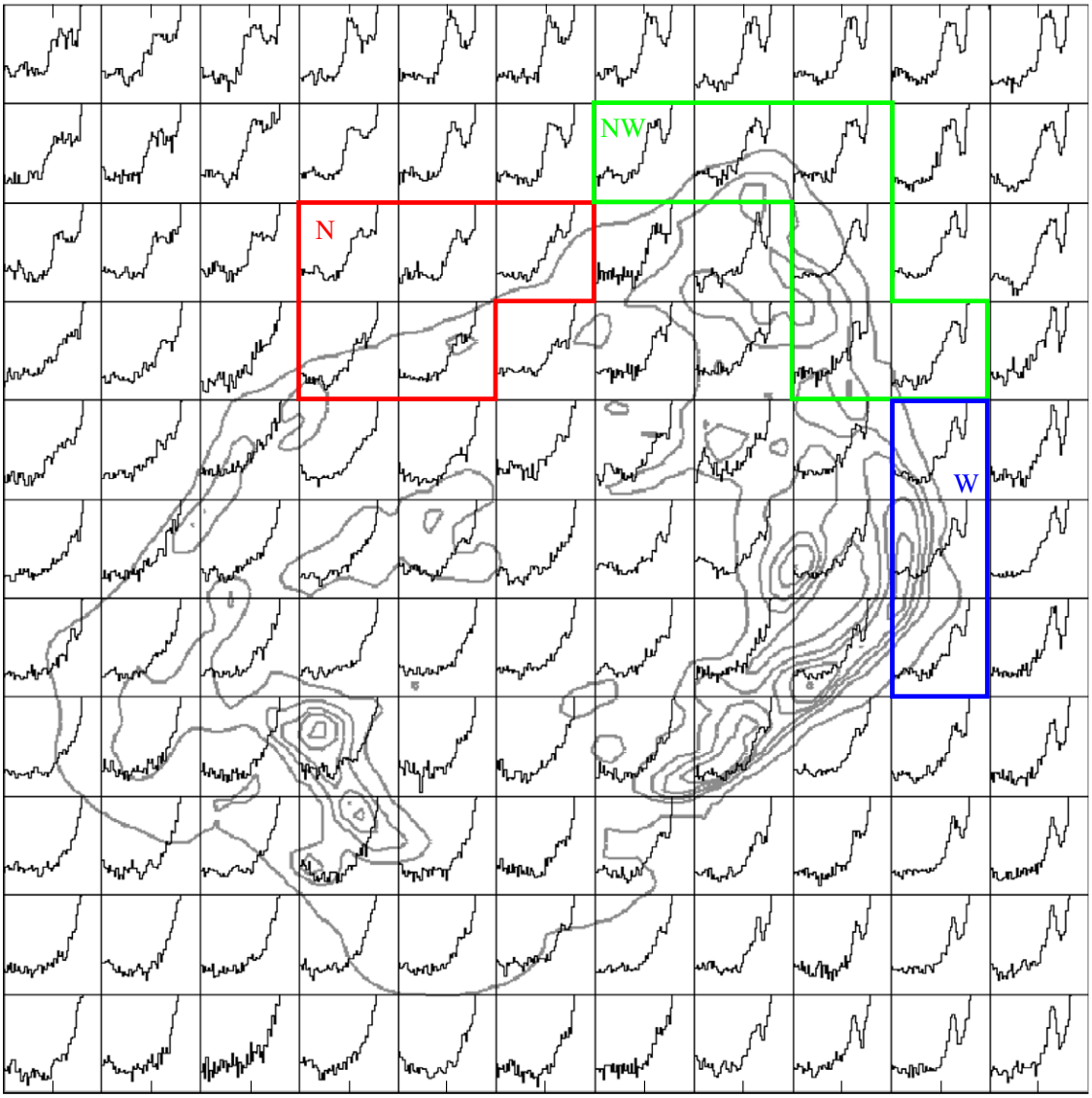

Figure 6. Grid of ^{12}CO ($J = 1$–0) spectra restricted to the velocity range 20–40 km s^{-1}, superposed on the VLA 1.4 GHz contours of 3C 397 remnant. Three regions ("N," "NW," and "W") are defined for CO-spectrum extraction, of which the 32 km s^{-1} ^{12}CO ($J = 1$–0) line profiles show broad blue wings (see Figure 7).

(A color version of this figure is available in the online journal.)

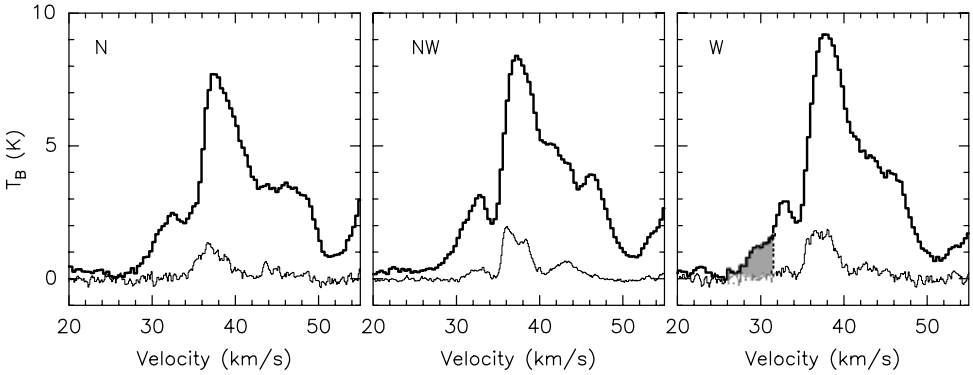

Figure 7. Averaged CO line profiles of the three regions marked in Figure 6. The ^{12}CO line profiles are plotted with thick lines and the ^{13}CO line profiles with thin lines. The shadowed patch indicates the blueward broadened wing of the ~32 km s^{-1} ^{12}CO component of region "W."

4. DISCUSSION

4.1. Mean Molecular Density

The H_2 column density distributions of the $V_{LSR} \sim 32$ km s^{-1} component along the Galactic latitude and longitude lines crossing the remnant center are plotted in Figure 8 (using the X-factor method). The H_2 column is shown to increase along the latitude toward the Galactic plane and has a depression within the SNR's extent ($\Delta N(H_2) \sim (0.3–1) \times 10^{21}$ cm^{-2}) along the longitude, corresponding to the molecular cavity. This

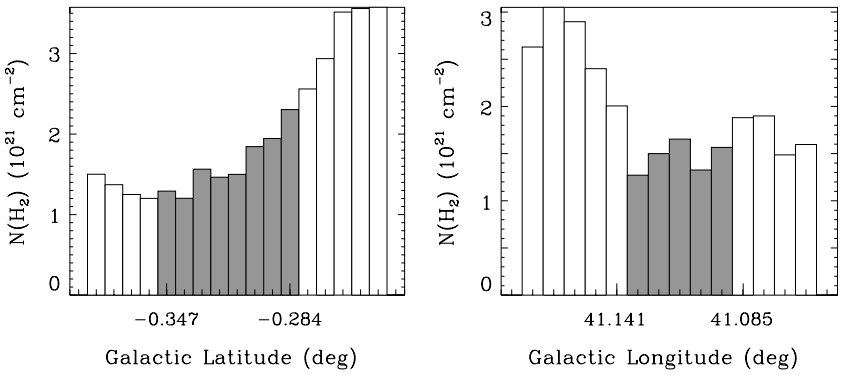

Figure 8. $N(H_2)$ distributions along the Galactic latitude (left panel) and longitude (right panel) lines projected across the remnant (shown in Figure 2). The gray bars indicate the extent of the remnant.

Table 1
Fitted and Derived Parameters for the MCs Around 32 km s^{-1} in Region "W"[a]

Gaussian components				
Line	Center (km s^{-1})	FWHM (km s^{-1})	T_{peak} (K)	W (K km s^{-1})
^{12}CO(J = 1–0)	32.7	2.5	2.9	7.7
^{13}CO(J = 1–0)	32.8	1.9	0.4	0.8
Molecular gas parameters				
	N (H_2) (10^{20} cm^{-2})	$M(M_\odot)$	T_{ex} (K)[b]	τ (^{13}CO)[c]
Gaussian components	13.9/11.1[d]	$197d^2_{10.3}/157d^2_{10.3}$[d]	8.8	0.17
Residual part[e]	5.2	$74d^2_{10.3}$		
Total (Gaussian+residual)	19.1	$271d^2_{10.3}$		

Notes.
[a] The region is marked in Figure 6.
[b] The excitation temperature calculated from the maximum ^{12}CO(J = 1–0) emission point of the 32 km s^{-1} component in the FOV.
[c] The optical depth of the ^{13}CO(J = 1–0).
[d] Two methods are applied for the estimates (see the text in Section 3.2).
[e] Determined by subtracting the Gaussian components centered at 32.7 km s^{-1} from the ^{12}CO emission in the velocity interval 27–34 km s^{-1} and applying the X-factor method.

column depression implies a mean density $n(H_2) \sim 10d_{10.3}^{-1}$–$30d_{10.3}^{-1}$ cm^{-3} for the molecular gas which was originally in the cavity. It can be roughly regarded as the mean density of the environs. Here we have assumed the line-of-sight length of the cavity as $10d_{10.3}$ pc, according to the $3\farcm2 \times 4\farcm7$ angular size of the rectangular-shaped SNR which converts to a physical extent of $\sim 9d_{10.3}$ pc $\times$ $14d_{10.3}$ pc. For comparison, the 32 km s^{-1} molecular component in the FOV has an average H_2 column density of $\sim 2.5 \times 10^{21}$ cm^{-2} (estimated from the first method) or $\sim 1.1 \times 10^{21}$ cm^{-2} (estimated from the second method), with the mass amounting to $3.0 \times 10^4\ M_\odot$ or $1.3 \times 10^4\ M_\odot$, respectively.

The column variation of the 32 km s^{-1} cloud along the latitude is as large as $\Delta N(H_2) \sim 1 \times 10^{21}$ cm^{-2}, but it cannot alone account for the variation of intervening hydrogen column density ($\Delta N_H \sim 1.1 \times 10^{22}$ cm^{-2}) from west to east inferred from the previous *Chandra* X-ray analysis (S05). On the other hand, the 38 km s^{-1} MC has a column density $N(H_2)$ $\sim 0.6 \times 10^{22}$ cm^{-2} (using the first method) or 0.34×10^{22} cm^{-2} (using the second method), which is well consistent with the variation of X-ray absorption. Therefore, the variation in absorption can basically be explained as a result of the presence of the 38 km s^{-1} MC, which partially covers the western and southern borders of the remnant.

4.2. Multi-wavelength Properties

Direct contact of the SNR with the MC can help us understand the other properties of the remnant. The pronounced 24 μm shell, correlating with the radio shell, follows the molecular cavity wall rather well. This mid-IR emission may be primarily due to the dust collisionally heated by electrons and ions in the outward moving shock wave as argued for the cases of, e.g., N132D (Tappe et al. 2006) and 3C 391 (Su & Chen 2008) where the blast wave has swept up dense material in those molecular environments. We refer the reader to A. Tappe et al. (2010, in preparation) for a detailed study of the IR properties of 3C 397.

S05 points out that 3C 397 bears some interesting similarities to the thermal composite (or mixed-morphology) SNR 3C 391 in radio and X-rays. The association of 3C 397 with the 32 km s^{-1} cloud demonstrates more similarities between the two SNRs. Both of them are observed to be located at the edge of a MC, align in a density gradient from SE to NW, and represent a "breakout" morphology in the east, resulting in bright radio shells in the NW and lower surface brightness in the SE.

The association of SNR 3C 397 with the MC enables us to explain the large volume emission measure of the low-temperature component of the X-ray emitting gas (Chen et al. 1999; Safi-Harb et al. 2000; S05). In fact, the molecular gas density

($\sim 10 d_{10.3}^{-1}$–$30 d_{10.3}^{-1}$ cm^{-3}) is similar to the ambient gas density inferred from the X-ray spectral analysis (Chen et al. 1999; Safi-Harb et al. 2000; S05). It has been suggested based on detailed *Chandra* X-ray spectroscopic analysis that the X-ray emission arises from low-ionization-timescale shock-heated ejecta mixed with shocked ambient/circumstellar material within a relatively young age of the remnant ~5.3 kyr (S05). If the molecular cavity was excavated by the supernova blast wave, the ejecta may be expected to have been fully mixed with the large-mass ($\sim 1 \times 10^3 d_{10.3} [n(\mathrm{H_2})/20\ \mathrm{cm^{-3}}]\ M_\odot$) of swept-up dense gas, so that it would be difficult to spectrally resolve metal-rich ejecta. If the cavity was sculpted chiefly by the progenitor star due to its powerful stellar wind and ionizing radiation, the ejecta would travel in the low-density region before impacting the dense molecular gas. Thus, the interaction of the ejecta with the dense ambient gas should be a recent event and hence the ionization timescale of the ejecta is naturally low. This wind cavity scenario seems to be in favor of the suggestion of reflected shock (S05) inside the SNR. The impact with the cavity wall may have hampered the expansion of the ejecta and, while the outermost ejecta can interact with the dense cloud, the innermost ejecta can be compressed and heated by the reflected shock (as happens, for example, in W49B (Miceli et al. 2006), in the Cygnus Loop (Levenson & Graham 2005), and in Kes 27 (Chen et al. 2008)). A detailed investigation of the X-ray properties of the remnant using *XMM-Newton* will be presented elsewhere (S. Safi-Harb et al. 2010, in preparation).

4.3. Multi-phase Molecular Environment

For the westmost line-broadened region, we adopt the observed total mass $\sim 270 d_{10.3}^2\ M_\odot$ and the Gaussian-subtracted mass $\sim 74 d_{10.3}^2\ M_\odot$ (Table 1) as the upper and lower limits of the mass of the disturbed molecular gas, respectively. Both estimates are larger than the mass, $18 d_{10.3}^2$–$54 d_{10.3}^2\ M_\odot$, of the molecular gas that could be swept up from the geometric center to this position (here we adopt one-fourth the volume of the cone subtended by the western boundary since region "W" shown in Figure 6 spans approximately half the western boundary and since only the one-sided line broadening is taken into account). On the other hand, we have mentioned that the original molecular gas in the cavity volume can roughly account for the low-temperature component of the X-ray emitting gas. Therefore, the disturbed gas in the line-broadened region is not swept-up gas but pre-exists there. The disturbed gas moves at a bulk velocity v_m around 7 km s^{-1}, which is implied by the blueward line broadening that reflects the velocity component along the line of sight. This motion can be naturally explained to be driven by the transmitted shock in dense clouds. The gas may thus be assumed to be in a crude pressure balance with the proximate hot gas, which will be represented in the following quantitative analysis by the "western lobe" described in S05. For the "western lobe," the assumption of pressure balance between the low-temperature component of hot gas ($kT_l \sim 0.2$ keV, with volume emission measure $4.2 \times 10^{60} d_{10.3}^2$ cm^{-3}; S05) and the high-temperature component ($kT_h \sim 1.4$ keV, with volume emission measure $6.2 \times 10^{57} d_{10.3}^2$ cm^{-3}; S05) yields values of filling factor and atomic density ($f_l \sim 0.94$, $n_l \sim 66 d_{10.3}^{-1/2}$ cm^{-3}) for the low-temperature component and ($f_h \sim 0.06$, $n_h \sim 10 d_{10.3}^{-1/2}$ cm^{-3}) for the high-temperature component. (The small filling factor of the high-temperature component seems to be consistent with the ejecta.) Here we have assumed $f_l + f_h = 1$ (Rho & Borkowski 2002), while in reality $f_l + f_h$ may be somewhat smaller than unity. However, because the hot gas density is proportional to the inverse of the square root of the filling factor, the density estimate is not sensitive to the factor. Hence the above density estimates are lower limits, but are still a good approximation. We thus find the density of the disturbed molecular gas $n(\mathrm{H_2}) \sim 2 \times 10^4 d_{10.3}^{-1/2}$ cm^{-3} based on the pressure balance between the cloud shock and the X-ray emitting hot gas (Zel'dovich & Raizer 1967; McKee & Cowie 1975): $1.4 \times 2 n(\mathrm{H_2}) m_H v_m^2 \sim 2.3 n_l k T_l$ ($\sim 2.3 n_h k T_h$). The derived high $n(\mathrm{H_2})$ value implies that the disturbed molecular gas is in very dense clumps. The co-existence of moderate-density ($\lesssim 100$ cm^{-3}) molecular component and dense clumps ($\sim 10^4$ cm^{-3}) illustrates a complicated multi-phase molecular environment in the west of SNR 3C 397. This is not uncommon; for example, similar multi-phase MCs have also been discovered in the western region of SNR 3C 391 (Reach & Rho 2000).

5. SUMMARY

We have presented an observation in millimeter CO lines toward the Galactic SNR 3C 397 which is characterized by an unusual rectangular morphology. The SNR is confined in a cavity of molecular gas at an LSR velocity of ~32 km s^{-1} and is embedded at the edge of the MC. The cloud has a column density gradient increasing from SE to NW, perpendicular to the Galactic plane, and in agreement with the elongation direction of the remnant. The ~32 km s^{-1} ^{12}CO line profiles with broad blue wings are demonstrated along the northern, northwestern, and westmost boundaries of the SNR; the blue wing of the westmost region may safely be ascribed to Doppler broadening and hence shows solid kinematic evidence for the disturbance by the SNR shock. The systemic velocity, 32 km s^{-1}, leads to a determination of kinematic distance of ~10.3 kpc to the cloud and SNR 3C 397. The mean molecular gas density of the SNR environment is estimated as $\sim 10 d_{10.3}^{-1}$–$30 d_{10.3}^{-1}$ cm^{-3}, consistent with the density of the ambient gas previously inferred from X-ray analyses, while the disturbed gas density is deduced as $\sim 10^4$ cm^{-3}, ascribed to very dense clumps, implicating a multi-component molecular environment there. Another MC along the line of sight at around 38 km s^{-1}, which was originally suggested to be associated with the remnant, may be instead located in front of the tangent point, at a distance of ~2.1 kpc, as implied by the H I SA. The variation of X-ray absorption from west to east revealed by S05 can basically be explained as a result of the presence of the 38 km s^{-1} MC, which partially covers the western and southern borders of the SNR. We compile a list of Galactic SNRs so far confirmed and suggested to be in physical contact with adjacent MCs in the Appendix.

We thank the anonymous referee for helpful comments. We are grateful to the staff of Qinghai Radio Observing Station at Delingha for help during the observation and to Lawrence Rudnick for providing the VLA data of SNR 3C 397. Fabrizio Bocchino and Estela Reynoso are appreciated for constructive help in improving the table of interacting SNRs. Y.C. acknowledges support from NSFC grants 10725312 and 10673003 and the 973 Program grant 2009CB824800. S.S.H. acknowledges support by the Natural Sciences and Engineering Research Council of Canada and the Canada Research Chairs program. We acknowledge the use of the VGPS data; the National Radio Astronomy Observatory is a facility of the National Science Foundation operated under cooperative agreement by Associated Universities, Inc. This research made

Table 2
Galactic SNRs in Physical Contact with MCs

Name	Other Name	Type[a]	Evidence[b]	Reference[c]	Group[d]	γ-ray detection[e](Reference[f])
G0.0+0.0	Sgr A East	TC	OH maser, CS MA & LB, H_2	1, 2, 3, 4, 5	Y	HESS(67)
G1.05–0.1	Sgr D SNR	S	OH maser	2, 6	Y	
G1.4–0.1		S	OH maser	2, 6	Y	
G5.4–1.2	Milne 56	C?	OH maser	7	Y	
G5.7–0.0		?	OH maser	7	Y	HESS(68)
G6.4–0.1	W28	TC	OH maser, CO MA & LB, H_2 MA, NIR	2, 8, 9, 10	Y	EGRET(69), HESS(68)
G8.7–0.1	W30	TC	OH maser	7	Y	HESS(70)
G9.7–0.0		S	OH maser	7	Y	
G16.7+0.1		C	OH maser, CO MA	2, 11, 12	Y	
G18.8+0.3	Kes 67	S	CO MA & LB, CO ratio	13, 14	Y	
G21.8–0.6	Kes 69	TC	OH maser, CO MA & LB, HCO^+, H_2	2, 11, 15, 16	Y	
G29.7–0.3	Kes 75	C	CO MA & LB	17	Y	
G31.9+0.0	3C 391	TC	OH maser, molecular MA & LB, H_2, NIR	2, 18, 19, 20	Y	
G32.8–0.1	Kes 78	S	OH maser	21	Y	
G34.7–0.4	W44	TC	OH maser, molecular LB, H_2 MA, NIR, CO ratio	2, 8, 10, 22	Y	EGRET(69)
G39.2–0.3	3C 396	C	H_2 & NIR MA, CO MA & LB	16, 23, 24	Y	
G41.1–0.3	3C 397	TC	CO MA & LB	25	Y	
G49.2–0.7	W51	TC	OH maser, CO MA & LB, HCO^+ LB	2, 11, 26	Y	HESS(71), Milagro(72)
G54.4–0.3	HC40	S	CO MA & LB, IR MA	27, 28	Y	
G89.0+4.7	HB21	TC	CO MA & LB, CO ratio, H_2, NIR	29, 30, 31	Y	
G109.1–1.0	CTB 109	S	CO MA & LB	32	Y	
G189.1+3.0	IC 443	TC	OH maser, CO ratio, H_2, molecular MA & LB	2, 8, 22, 33, 34, 35	Y	EGRET(69), MAGIC(73) Milagro(72), VERITAS(74) AGILE(75)
G304.6+0.1	Kes 17	S	H_2, IR MA & colors	16, 28	Y	
G332.4–0.4	RCW 103	S	IR MA & colors, NIR, H_2 & HCO^+ MA	28, 36, 37	Y	
G337.0–0.1	CTB 33	S	OH maser	18	Y	
G337.8–0.1	Kes 41	S	OH maser	21	Y	
G346.6–0.2		S	OH maser, H_2, IR colors	21, 16, 28	Y	
G347.3–0.5		S?	CO MA & LB	38	Y	CANGAROO(76) HESS(77), Fermi(78)
G348.5–0.0		S?	OH maser, H_2, IR MA	2, 16, 28	Y	
G348.5+0.1	CTB 37A	S	OH maser, CO MA	2, 12, 18	Y	HESS(79)
G349.7+0.2		S	OH maser, CO MA & LB, CO ratio, H_2, IR MA	2, 18, 13, 16, 28	Y	
G357.7+0.3	Square Nebula	S	OH maser	2, 6	Y	
G357.7–0.1	MSH 17–39	TC	OH maser, CO & H_2 MA	2, 18, 39	Y	
G359.1–0.5		TC	OH maser, CO & H_2 MA	2, 40, 41, 42	Y	HESS(80)
G33.6+0.1	Kes 79	TC	CO MA, HCO^+ MA	43	Y?	
G40.5–0.5		S	CO MA	44	Y?	Milagro(81), HESS(82)
G43.3–0.2	W49B	TC	H_2 MA	45	Y?	
G54.1+0.3		F?	CO MA	46	Y?	
G74.0–8.5	Cygnus Loop	S	CO MA	47	Y?	
G78.2+2.1	γ Cygni SNR	S	CO MA	48	Y?	EGRET(83), Milagro(81)
G84.2–0.8		S	CO MA	49, 50	Y?	
G120.1+1.4[g]	Tycho, SN1572	S	CO MA	51	Y?	
G132.7+1.3	HB3	TC	CO MA	52	Y?	EGRET(83)
G263.9–3.3	Vela	C	CO MA	53	Y?	CANGAROO(84) HESS(85)
G284.3–1.8	MSH 10–53	S	CO MA & possible LB	54	Y?	
G11.2–0.3		C	IR MA & colors	28	?	
G22.7–0.2		S	IR RC	28	?	
G23.3–0.3	W41	S	CO RC	55	?	HESS(67, 70, 86), MAGIC(87)
G39.7–2.0	W50, SS433	?	CO RC	56	?	
G63.7+1.1		F	CO RC	57	?	
G74.9+1.2	CTB 87	F	CO RC	49, 58, 59	?	
G94.0+1.0	3C434.1	S	CO RC	49	?	
G106.3+2.7		C?	CO RC	60	?	EGRET(83), Milagro(81), VERITAS(88)
G111.7–2.1	Cas A, 3C461	S	H_2CO absorption, CO RC	61, 62	?	HEGRA(89), MAGIC(90), VERITAS(91), Fermi(92)
G160.4+2.8	HB9	S	CO RC	49	?	
G166.0+4.3	VRO 42.05.01	TC	CO RC	49	?	
G166.3+2.5	OV 184	?	CO RC	49	?	

Table 2
(Continued)

Name	Other Name	Type[a]	Evidence[b]	Reference[c]	Group[d]	γ-ray detection[e](Reference[f])
G192.8–1.1	PKS 0607+17	S	CO RC	49	?	
G205.5+0.5	Monoceros Nebula	S	CO RC	63	?	EGRET(83), HESS (93)
G260.4–3.4	Puppis A	S	CO RC	64, 65	?	
G290.1–0.8	MSH 11-61A	TC	CO RC	66	?	
G310.8–0.4	Kes 20A	S	IR RC & colors	28	?	
G311.5–0.3		S	IR MA & colors	28	?	
G344.7–0.1		C?	IR RC & colors	28	?	

Notes.

[a] Types of SNRs — S: shell type; C: composite type; F: plerion (Crab-like) type; TC: thermal composite (Jones et al. 1998) (i.e., mixed-morphology, Rho & Petre 1998) type; ?: not classified or not sure yet.

[b] See the text in the Appendix for explanations.

[c] References.—(1) Yusef-Zadeh et al. 1996; (2) Hewitt et al. 2008; (3) Serabyn et al. 1992; (4) Yusef-Zadeh et al. 2001; (5) Lee et al. 2008; (6) Yusef-Zadeh et al. 1999; (7) Hewitt & Yusef-Zadeh 2009; (8) Claussen et al. 1997; (9) Arikawa et al. 1999; (10) Reach et al. 2005; (11) Green et al. 1997; (12) Reynoso & Mangum 2000; (13) Dubner et al. 2004; (14) Tian et al. 2007b; (15) Zhou et al. 2009; (16) Hewitt et al. 2009; (17) Su et al. 2009; (18) Frail et al. 1996; (19) Reach & Rho 1999; (20) Reach et al. 2002; (21) Koralesky et al. 1998; (22) Seta et al. 1998; (23) Lee et al. 2009; (24) Su et al. 2010, in preparation; (25) this work; (26) Koo & Moon 1997; (27) Junkes et al. 1992; (28) Reach et al. 2006; (29) Koo et al. 2001; (30) Byun et al. 2006; (31) Shinn et al. 2009; (32) Sasaki et al. 2006; (33) Rosado et al. 2007; (34) Turner et al. 1992; (35) Zhang et al. 2010; (36) Oliva et al. 1999; (37) Paron et al. 2006; (38) Moriguchi et al. 2005; (39) Lazendic et al. 2004; (40) Uchida et al. 1992; (41) Yusef-Zadeh et al. 1995; (42) Lazendic et al. 2002; (43) Green & Dewdney 1992; (44) Yang et al. 2006; (45) Keohane et al. 2007; (46) Leahy et al. 2008; (47) Scoville et al. 1977; (48) Fukui & Tatematsu 1988; (49) Huang & Thaddeus 1986; (50) Feldt & Green 1993; (51) Lee et al. 2004; (52) Routledge et al. 1991; (53) Moriguchi et al. 2001; (54) Ruiz & May 1986; (55) Leahy & Tian 2008; (56) Huang et al. 1983; (57) Wallace et al. 1997; (58) Cho et al. 1994; (59) Kothes et al. 2003; (60) Kothes et al. 2001; (61) Reynoso & Goss 2002; (62) Hines et al. 2004; (63) Oliver et al. 1996; (64) Dubner et al. 1988; (65) Paron et al., 2008; (66) Filipovic et al. 2005.

[d] Group: classification with "Y" as confirmed ones, "Y?" as probable ones, and "?" as possible ones.

[e] γ-ray detection: any γ-ray detection towards SNRs by various γ-ray detectors, such as HESS, EGRET, Milagro, MAGIC, VERITAS, HEGRA and *Fermi*.

[f] References.—(67) Aharonian et al. 2006a; (68) Aharonian et al. 2008a; (69) Esposito et al. 1996; (70) Aharonian et al. 2005; (71) Feinstein et al. 2008; (72) Abdo et al. 2009; (73) Albert et al. 2007a; (74) Acciari et al. 2009a; (75) Tavani et al. 2010; (76) Muraishi et al. 2000; (77) Aharonian et al. 2004; (78) Funk 2009; (79) Aharonian et al. 2008c; (80) Aharonian et al. 2008b; (81) Abdo et al. 2007; (82) Aharonian et al. 2009; (83) Casandjian & Grenier 2008; (84) Katagiri et al. 2005; (85) Aharonian et al. 2006b; (86) Tian et al. 2007a; (87) Albert et al. 2006; (88) Acciari et al. 2009b; (89) Aharonian et al. 2001; (90) Albert et al. 2007b; (91) Humensky et al. 2009; (92) Abdo et al. 2010; (93) Aharonian et al. 2007.

[g] Remnant of Type Ia supernova explosion.

use of NASA's Astrophysics Data System and of the High-energy Astrophysics Science Archive Research Center operated by NASA's Goddard Space Flight Center.

APPENDIX

GALACTIC SNRs IN CONTACT WITH MCs

Table 2 shows a compilation of Galactic SNRs that are presently known and suggested to be in physical contact with MCs. The evidence for the contact/interaction adopted in the table includes

1. detection of 1720 MHz OH maser within the extent of SNR;
2. presence of molecular (CO, HCO^+, CS, etc.) line broadening or asymmetric profile (LB);
3. presence of line emission with high high-to-low excitation line ratio, e.g., ^{12}CO $J = 2$–$1/J = 1$–0;
4. detection of near-infrared (NIR) emission, e.g., [Fe II] line or vibrational/rotational lines of H_2 (e.g., H_2 1–0 S(1) line (2.12 μm), H_2 0–0 S(0)–S(7) lines) due to shock excitation;
5. specific infrared (IR) colors suggesting molecular shocks, e.g., *Spitzer* IRAC 3.6 μm/8 μm, 4.5 μm/8 μm, and 5.8 μm/8 μm (Reach et al. 2006);
6. morphological agreement (MA) or correspondence of molecular features with SNR features (e.g., arc, shell, interface, etc.).

Condition 1 has been known as a reliable signpost of interacting SNRs and the combination of condition 6 and one of conditions 2–5 is now also accepted as convincing evidence for SNR–MC interaction. Condition 6 alone is, however, indicative of probable contact. Either of condition 5 and rough spatial coincidence (RC) between SNR and molecular features is suggestive of possible contact. The SNRs listed in Table 2 are thus classified into three groups: 34 confirmed ones ("Y"), 11 probable ones ("Y?") with strong evidence but not conclusive yet, and 19 possible ones ("?") remaining to be determined with further observations. Note that Tycho SNR is the only known Type Ia SNR in the table.

Since SNR–MC interaction is an important source of γ-ray emission via decay of pions, γ-ray detections along the line of sight are also listed in the table.

REFERENCES

Abdo, A. A., & Milagro Collaboration, 2007, ApJ, 664, L91
Abdo, A. A., & Milagro Collaboration, 2009, ApJ, 700, L127
Abdo, A. A., et al. 2010, ApJ, 710, L92
Acciari, V. A., & VERITAS Collaboration, 2009a, ApJ, 698, L133
Acciari, V. A., & VERITAS Collaboration, 2009b, ApJ, 703, L6
Aharonian, F., & HESS Collaboration, 2004, Nature, 432, 75
Aharonian, F., & HESS Collaboration, 2005, Science, 307, 1938
Aharonian, F., & HESS Collaboration, 2006a, ApJ, 636, 777
Aharonian, F., & HESS Collaboration, 2006b, A&A, 448, L43
Aharonian, F., & HESS Collaboration, 2007, A&A, 469, L1
Aharonian, F., & HESS Collaboration, 2008a, A&A, 481, 401
Aharonian, F., & HESS Collaboration, 2008b, A&A, 483, 509
Aharonian, F., & HESS Collaboration, 2008c, A&A, 490, 685
Aharonian, F., & HESS Collaboration, 2009, A&A, 499, 723
Aharonian, F., et al. 2001, A&A, 370, 112
Albert, J., & MAGIC Collaboration, 2006, ApJ, 643, L53
Albert, J., & MAGIC Collaboration, 2007a, ApJ, 664, L87
Albert, J., & MAGIC Collaboration, 2007b, A&A, 474, 937
Anderson, M. C., & Rudnick, L. 1993, ApJ, 408, 514

Arikawa, Y., Tatematsu, K., Sekimoto, Y., & Takahashi, T. 1999, PASJ, 51, L7
Byun, D., Koo, B., Tatematsu, K., & Sunada, K. 2006, ApJ, 637, 283
Casandjian, J.-M., & Grenier, I. A. 2008, A&A, 489, 849
Caswell, J. L., Murray, J. D., Roger, R. S., Cole, D. J., & Cooke, D. J. 1975, A&A, 45, 239
Chen, Y., Seward, F. D., Sun, M., & Li, J. T. 2008, ApJ, 676, 1040
Chen, Y., Sun, M., Wang, Z. R., & Yin, Q. F. 1999, ApJ, 520, 737
Cho, S., Kim, K. T., & Fukui, Y. 1994, AJ, 108, 634
Claussen, M. J., Frail, D. A., Goss, W. M., & Gaume, R. A. 1997, ApJ, 489, 143
Clemens, D. P. 1985, ApJ, 295, 422
Cox, A. N. (ed.) 2000, Allen's Astrophysical Quantities (New York: AIP)
Dame, T. M., Hartmann, D., & Thaddeus, P. 2001, ApJ, 547, 792
Dubner, G., Giacani, E., Reynoso, E., & Paron, S. 2004, A&A, 426, 201
Dubner, G. M., & Arnal, E. M. 1998, A&AS, 75, 363
Dyer, K. K., & Reynolds, S. P. 1999, ApJ, 526, 365
Esposito, J. A., Hunter, S. D., Kanbach, G., & Sreekumar, P. 1996, ApJ, 461, 820
Feinstein, F., Fiasson, A., Gallant, Y., Chaves, R. C. G., Marandon, V., de Naurois, M., Kosack, K., & Rowellf, G. 2008, in AIP Conf. Proc. 1112, Proc. 6th Science with the New Generation of High Energy Gamma-Ray Experiments, ed. D. Bastieri & R. Rando (Melville, NY: AIP), 54
Feldt, C., & Green, D. A. 1993, A&A, 274, 421
Filipovic, M. D., Payne, J. L., & Jones, P. A. 2005, Serb. Astron. J., 170, 47
Frail, D. A., Goss, W. M., Reynoso, E. M., Giacani, E. B., Green, A. J., & Otrupcek, R. 1996, AJ, 111, 1651
Frerking, M. A., Langer, W. D., & Wilson, R. W. 1982, ApJ, 262, 590
Fukui, Y., & Tatematsu, K. 1988, in IAU Colloq. 101, Supernova Remnants and Interstellar Medium, ed. R. S. Roger & T. L. Landecker (Cambridge: Cambridge Univ. Press), 261
Funk, S. 2009, Fermi Symposium 2009, Washington, DC, http://fermi.gsfc.nasa.gov/science/symposium/2009/abs/sfunk.html
Green, A. J., Frail, D. A., Goss, W. M., & Otrupeced, R. 1997, AJ, 114, 2058
Green, D. A., & Dewdney, P. E. 1992, MNRAS, 254, 686
Hewitt, J. W., Rho, J., Andersen, M., & Reach, W. T. 2009, ApJ, 694, 1266
Hewitt, J. W., & Yusef-Zadeh, F. 2009, ApJ, 694, L16
Hewitt, J. W., Yusef-Zadeh, F., & Wardle, M. 2008, ApJ, 683, 189
Hines, D. C., et al. 2004, ApJS, 154, 290
Huang, Y.-L., Dame, T. M., & Thaddeus, P. 1983, ApJ, 272, 609
Huang, Y.-L., & Thaddeus, P. 1986, ApJ, 309, 804
Humensky, T. B. (for the VERITAS Collaboration). 2009, Proc. of the 2009 Fermi Symposium, eConf C091122 (2009), arXiv:0912.4304
Jackson, J. M., Bania, T. M., Simon, R., Kolpak, M., Clemans, D. P., & Heyer, M. 2002, ApJ, 566, L81
Jiang, B., & Chen, Y. 2010, Sci. China Phys. Mech. Astron. Supplement, 53, 267
Jones, T. W., et al. 1998, PASP, 110, 125
Junkes, N., Furst, E., & Reich, W. 1992, A&AS, 96, 1
Katagiri, H., et al. 2005, ApJ, 619, L163
Keohane, J. W., Reach, W. T., Rho, J., & Jarrett, T. H. 2007, ApJ, 654, 938
Koo, B.-C., & Moon, D.-S. 1997, ApJ, 485, 263
Koo, B.-C., Rho, J., Reach, W. T., Jung, J. H., & Mangum, J. G. 2001, ApJ, 552, 175
Koralesky, B., Frail, D. A., Goss, W. M., Claussen, M. J., & Green, A. J. 1998, AJ, 116, 1323
Kothes, R., Reich, W., Foster, T., & Byun, D. 2003, ApJ, 588, 852
Kothes, R., Uyaniker, B., & Pineault, S. 2001, ApJ, 560, 236
Landecker, T. L., Routledge, D., Reynolds, S. P., Smegal, R. J., Borkowski, K. J., & Seward, F. D. 1999, ApJ, 527, 866
Lazendic, J. S., Wardle, M., Burton, M. G., Yusef-Zadeh, F., Green, A. J., & Whiteoak, J. B. 2004, MNRAS, 354, 393
Lazendic, J. S., Wardle, M., Burton, M. G., Yusef-Zadeh, F., Whiteoak, J. B., Green, A. J., & Ashley, M. C. B. 2002, MNRAS, 331, 537
Leahy, D. A., & Tian, W. W. 2008, AJ, 135, 167
Leahy, D. A., Tian, W. W., & Wang, Q. D. 2008, AJ, 136, 1477
Lee, H., Moon, D., Koo, B., Lee, J., & Matthews, K. 2009, ApJ, 691, 1042
Lee, J., Koo, B., & Tatematsu, K. 2004, ApJ, 605, L113
Lee, S., et al. 2008, ApJ, 674, 247
Levenson, N. A., & Graham, J. R. 2005, ApJ, 622, 366
Liszt, H. S., Burton, W. B., & Bania, T. M. 1981, ApJ, 246, 74
McKee, C. F., & Cowie, L. L. 1975, ApJ, 195, 715
Miceli, M., Decourchelle, A., Ballet, J., Bocchino, F., Hughes, J. P., Hwang, U., & Petre, R. 2006, A&A, 453, 567
Moriguchi, Y., Tamura, K., Tawara, Y., Sasago, H., Yamaoka, K., Onishi, T., & Fukui, Y. 2005, ApJ, 631, 947
Moriguchi, Y., Yamaguchi, N., Onishi, T., Mizuno, A., & Fukui, Y. 2001, PASJ, 53, 1025
Muraishi, H., et al. 2000, A&A, 354, L57
Oliva, E., Moorwood, A. F. M., Drapatz, S., Lutz, D., & Sturm, E. 1999, A&A, 343, 943
Oliver, R. J., Masheder, M. R. W., & Thaddeus, P. 1996, A&A, 315, 578
Paron, S., Dubner, G., Reynoso, E., & Rubio, M. 2008, A&A, 480, 439
Paron, S. A., Reynoso, E. M., Purcell, C., Dubner, G. M., & Green, A. 2006, PASA, 23, 69
Radhakrishnan, V., Goss, W. M., Murray, J. D., & Brooks, J. W. 1972, ApJS, 24, 49
Reach, W. T., & Rho, J. H. 1999, ApJ, 511, 836
Reach, W. T., & Rho, J. H. 2000, ApJ, 544, 843
Reach, W. T., Rho, J., & Jarrett, T. H. 2005, ApJ, 618, 297
Reach, W. T., Rho, J., Jarrett, T. H., & Lagage, P. O. 2002, ApJ, 564, 302
Reach, W. T., et al. 2006, AJ, 131, 1479
Reid, M. J. 1993, ARA&A, 31, 345
Reynoso, E. M., & Goss, W. M. 2002, ApJ, 575, 871
Reynoso, E. M., & Mangum, J. G. 2000, ApJ, 545, 874
Reynoso, E. M., & Mangum, J. G. 2001, AJ, 121, 347
Rho, J., & Bowkowski, K. J. 2002, ApJ, 575, 201
Rho, J., & Petre, P. 1998, ApJ, 503, L167
Roman-Duval, J., Jackson, J. M., Heyer, M., Johnson, A., Rathborne, J., Shah, R., & Simon, R. 2009, ApJ, 699, 1153
Rosado, M., Arias, L., & Ambrocio-Cruz, P. 2007, AJ, 133, 89
Routledge, D., Dewdney, P. E., Landecker, T. L., & Vaneldik, J. F. 1991, A&A, 247, 529
Ruiz, M. T., & May, J. 1986, ApJ, 309, 667
Safi-Harb, S., Dubner, G., Petre, R., Holt, S. S., & Durouchoux, P. 2005, ApJ, 618, 321 (S05)
Safi-Harb, S., Petre, R., Arnaud, K. A., Keohane, J. W., Borkowski, K. J., Dyer, K. K., Reynolds, S. P., & Hughes, J. P. 2000, ApJ, 545, 922
Sasaki, M., Kothes, R., Plucinsky, P., Gaetz, T. J., & Brunt, C. M. 2006, ApJ, 642, L149
Scoville, N. Z., Irvine, W. M., Wannier, P. G., & Predmore, C. R. 1977, ApJ, 216, 320
Serabyn, E., Lacy, J. H., & Achtermann, J. M. 1992, ApJ, 395, 166
Seta, M., et al. 1998, ApJ, 505, 286
Shinn, J., Koo, B., Burton, M. G., Lee, H., & Moon, D. 2009, ApJ, 693, 1883
Stil, J. M., et al. 2006, AJ, 132, 1158
Su, Y., & Chen, Y. 2008, AdSpR, 41, 401
Su, Y., Chen, Y., Yang, J., Koo, B. C., Zhou, X., Jeong, I. G., & Zhang, C. G. 2009, ApJ, 694, 376
Tappe, A., Rho, J., & Reach, W. T. 2006, ApJ, 653, 267
Tavani, M., & AGILE Collaboration. 2010, ApJ, 710, L151
Tian, W. W., Leahy, D. A., & Wang, Q. D. 2007a, A&A, 474, 541
Tian, W. W., Li, Z., Leahy, D. A., & Wang, Q. D. 2007b, ApJ, 657, L25
Turner, B. E., Chan, K., Green, S., & Lubowich, D. A. 1992, ApJ, 399, 114
Uchida, K. I., Morris, M., Bally, J., Pound, M., & Yusef-Zadeh, F. 1992, ApJ, 398, 128
Wallace, B. J., Landecker, T. L., & Taylor, A. R. 1997, AJ, 114, 206
White, G. J., Rainey, R., Hayashi, S. S., Saeko, S., & Kaifu, N. 1987, A&A, 173, 337
Yang, J., Zhang, J. L., Cai, Z. Y., Lu, D. R., & Tan, Y. H. 2006, Chin. J. Astron. Astrophys., 6, 210
Yusef-Zadeh, F., Goss, W. M., Roberts, D. A., Robinson, B., & Frail, D. A. 1999, ApJ, 527, 172
Yusef-Zadeh, F., Roberts, D. A., Goss, W. M., Frail, D. A., & Green, A. J. 1996, ApJ, 466, L25
Yusef-Zadeh, F., Stolovy, S. R., Burton, M.,, & Ashley, M. C. B. 2001, ApJ, 560, 749
Yusef-Zadeh, F., Uchida, K. I., & Roberts, D. 1995, Science, 270, 1801
Zel'dovich, Ya. B., & Raizer, Yu. M. 1967, Physics of Shock Waves and High-Temperature Hydrodynamic Phenomena (New York: Academic)
Zhang, Z., Gao, Y., & Wang, J. 2010, Sci. China Phys. Mech. Astron., in press arXiv:0911.4815
Zhou, X., Chen, Y., Su, Y., & Yang, J. 2009, ApJ, 691, 516